ELSEVIER

Physics of the Earth and Planetary Interiors 120 (2000) 11–27

PHYSICS OF THE EARTH AND PLANETARY INTERIORS

www.elsevier.com/locate/pepi

Paleomagnetism and magnetic fabric of Middle Jurassic dykes from Western Patagonia, Argentina

Augusto E. Rapalini [a,*], Mónica Lopez de Luchi [b]

[a] *Laboratorio de Paleomagnetismo Daniel Valencio, Departamento de Ciencias Geológicas, FCEyN, Universidad de Buenos Aires, Pabellón 2, Ciudad Universitaria, 1428 Buenos Aires, Argentina*

[b] *Centro de Investigaciones en Recursos Geológicos, CONICET, Ramirez de Velasco 847, 1414 Buenos Aires, Argentina*

Received 15 June 1998; received in revised form 15 June 1999; accepted 10 January 2000

Abstract

Jurassic volcanism in Patagonia is widespread. Although associated dyke swarms are conspicuous, they have been almost neglected in previous geologic studies of this region. Radiometric, paleomagnetic and magnetic anisotropy studies are reported from a Middle Jurassic basic to intermediate dyke swarm exposed in the Sierra de Mamil Choique (Western Patagonia) in an area of over 350 km^2. Two whole-rock K/Ar determinations indicate that these dykes were intruded at around 170 Ma. An anisotropy of magnetic susceptibility (AMS) study on 15 dykes (74 block samples) shows that they carry different kinds of magnetic fabric (both normal and inverse), apparently governed by compositional differences. A paleomagnetic study of these samples suggests that Ti-poor titanomagnetite is the probable carrier of the characteristic remanence. Mean site characteristic directions pass a reversal test (grade C). A paleomagnetic pole, computed by averaging VGPs from each individual dyke, is situated at 70.2°S, 190.4°E ($N = 13$, $\alpha_{95} = 9.7°$), not substantially apart from other Middle Jurassic poles from South America. Further refinement of the Jurassic South American apparent polar wander path is needed to establish whether or not the Mamil Choique dykes were affected by a small tectonic rotation.

Keywords: Paleomagnetism; Magnetic fabric; Dyke swarms; Patagonia; South America; Jurassic

1. Introduction

The Jurassic has been considered for a long time as a period of small, perhaps negligible, apparent polar wander for South America. Several authors have proposed or assumed a quasi-static period for South America during most of the Jurassic, which may have begun as early as Late Permian (Valencio et al., 1983; Beck, 1988; Rapalini et al., 1993). However, this view has been challenged recently by others (Vizán, 1993; Iglesia Llanos, 1997) who argue in favor of apparent polar wander of South America in the Jurassic, similar, in a way, to previous suggestions by Irving and Irving (1982). All these interpretations are hampered by the fact that paleomagnetic data for the Jurassic of this continent are scarce, many of the poles being of questionable reliability

* Corresponding author. Fax: +54-11-4576-3329.

E-mail addresses: rapalini@gl.fcen.uba.ar (A.E. Rapalini), deluchi@mail.retina.ar (M. Lopez de Luchi).

0031-9201/00/$ - see front matter
PII: S0031-9201(00)00140-0

and their ages sometimes not very well constrained. These arguments are sufficient to justify carrying out new paleomagnetic studies on well-dated Jurassic rocks in South America. Patagonia is among the best South American regions for paleomagnetic research on Jurassic magmatic rocks because several large Jurassic igneous provinces are very well exposed.

Middle Jurassic volcanism of Patagonia has been widely studied as it represents a major magmatic event in the evolution of this region (Lesta and Ferello,1972; Nullo, 1978; Page and Page, 1993; Pankhurst and Rapela, 1995; Pankhurst et al., 1993 Rapela and Pankhurst, 1993). The Mesozoic acid volcanic province of Patagonia (Gust et al., 1985) covers an area of about 1 million km^2 and has been subdivided into two complexes, Marifil in the eastern sector of the North Patagonian Massif (NPM) and Chon-Aike in the eastern sector of the Deseado Massif (DM, Fig. 1 inset). Mainly basic to intermediate volcanism developed west of these areas and is represented by the Taquetrén and Cañadón Asfalto Formations and the Lonco Trapial Group in NPM and by the Bajo Pobre Formation in DM (Pankhurst et al., 1993; Pankhurst and Rapela, 1995; Rapela and Pankhurst, 1993). This volcanism, considered as part of the Patagonian Central Volcanic Belt (CVB, Page and Page, 1993), is composed of pyroxene–amphibole andesitic to dacitic lava flows and breccias associated with eroded subvolcanic units. A north to south migration of the volcanic activity has been proposed for the acid volcanism, with the Marifil Complex restricted to 178–183 Ma and the Chon-Aike Complex to 168–170 Ma (Pankhurst et al., 1993; Pankhurst and Rapela, 1995; Rapela and Pankhurst, 1993). Age determinations for the CVB are fewer and more scattered, with ages ranging from 136 to 180 Ma. (Lesta and Ferello,1972; Nullo, 1978; Page and Page, 1993; Alric et al., 1996). This fact has contributed to unclear stratigraphic relationships between some of these units in certain areas. A western migration of the volcanic activity with younger less siliceous compositions also has been proposed (Pankhurst and Rapela, 1995). While the extensive silicic volcanism in eastern Patagonia was

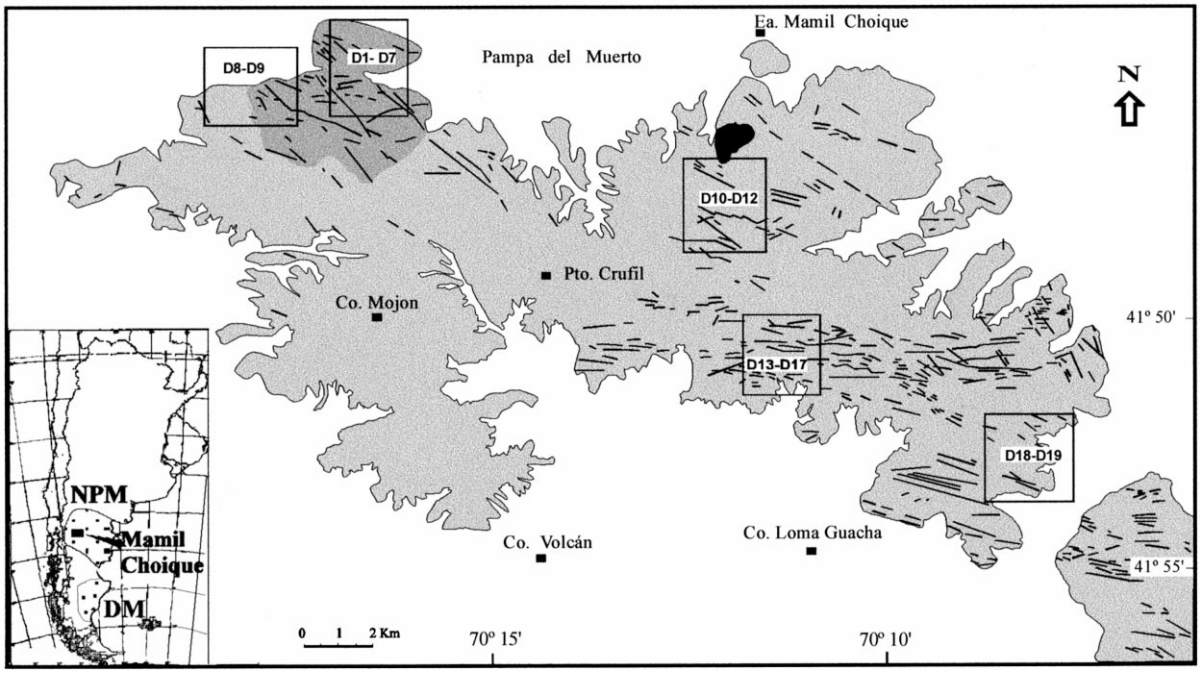

Fig. 1. Geological map of the Sierra de Mamil Choique and location of sampling sites for radiometric, paleomagnetic and AMS studies. Light grey: Mamil Choique granotoids; dark grey: Viuda del Gallo granite; black: La Pintada granite; white: Cenozoic deposits. NPM: North Patagonian massif; DM: Deseado massif. More references and discussion in the text.

interpreted as the product of an extensional tectonic setting, associated with the rifting and incipient break up of Gondwana (Pankhurst and Rapela, 1995), the mesosilicic to basic volcanic rocks of the CVB have been assigned to an eastern branch of the Jurassic Volcanic Arc (Page and Page, 1993).

Dyke swarms intruding basement rocks are useful in order to understand the brittle behaviour of the upper continental crust as a response to tectonic processes. Although basic to intermediate dyke swarms are common in NPM, they have been seldom studied and no precise relation with the major volcanic events that characterize the Mesozoic and Tertiary magmatism of Patagonia have been proposed.

The Sierra de Mamil Choique (SW Rio Negro Province, Argentina, Lopez de Lucchi and Rapalini, 1997; Fig. 1), recently, has been the focus of combined geologic, lithologic, geochemical, radiometric, paleomagnetic and magnetic fabric studies. Results from application of the latter three methods to the Mamil Choique dyke swarm are presented in this contribution.

2. Geology of the area

The dyke swarm under study is located in the Sierra de Mamil Choique (41°40′–41°55′S and 70°–70°33′W) and the smaller satellite hills to the north (Fig. 1), although it clearly extends — as the same or associated swarm — out of the study area, through the Sierra del Medio (~50 km to the SE). The Lower Paleozoic basement of the Sierra de Mamil Choique is composed of the Early Paleozoic (?) metamorphic Cushamen Formation (CF, Ravazzoli and Sesana, 1977; Dalla Salda et al., 1994, López de Luchi and Cerredo, 1996), the intrusive Upper Ordovician–Lower Silurian Mamil Choique Granitoids (MCG) (Dalla Salda et al. 1994), the recently described Tunnel Tonalites (TT) (López de Luchi and Cerredo, 1996) and the Devonian Viuda de Gallo (VDG) granitoids (Dalla Salda et al., 1994). The pre-MCG evolution is related to the medium pressure regional metamorphism of the CF. Metamorphism affected a siliciclastic pile with some thin acid and basic volcanic interlayers. The MCG were emplaced, postdating regional metamorphism. The TT and MCG could be ascribed to the same tectonothermal event. Regional relationships among metamorphism–deformation–magmatism agree with what is to be expected from a collisional setting, with peak metamorphic conditions being synchronous with the second deformation and with magmatism postdating regional metamorphism (López de Luchi and Cerredo, 1996, Cerredo and López de Luchi, 1998). The Upper Permian La Pintada (LPG) granitoids appear as scattered minor outcrops.

Radiometric dating of the dyke swarm at Sierra de Mamil Choique was lacking before this study. Furthermore, stratigraphic control of its age was very loose, as it only indicated a post-Devonian age with no upper limit. The Permian LPG, apparently not intruded by the dykes, is exposed in small restricted outcrops somewhat separated from the area affected by the dykes.

3. Lithology, geochemical characterization and age of the dykes

These dykes are composed of dark green to greenish grey basalts, basaltic andesites, basaltic trachyandesites, trachyandesites, and, in a few cases, reddish grey dacites. Dykes are vertical; their thicknesses vary from 1 to 6 m and they may be up to 3 km long, albeit discontinuous in outcrop. They are fine grained with affanitic to very-fine-grained mesostasis. Textures vary from porphyric to aphyric types with a broadly defined zonal pattern with increasing porphyric textures (phenocryst (%): 15–60) and grain size towards the central part of the widest dykes (i.e., 6 m). Broadly speaking, the highest phenocryst percentages are linked to andesitic compositions with scarce mafites as phenocrysts. In the porphyric facies, at least three phenocryst associations have been recognised: clinopyroxene–plagioclase ± clinoamphibole for the basaltic andesites; plagioclase–clinoamphibole for the basaltic trachyandesites and trachyandesites and plagioclase both in the basaltic andesites and in the trachyandesites. Accessory minerals include interstitial quartz and alkali feldspar in some andesites, and apatite, which is always restricted to the mesostasis. Opaque content varies from 15% to 5% in the mesostasis, and it constitutes no more than 3% as bigger subhedral crystals associated with altered mafites in basalts. Higher opaque

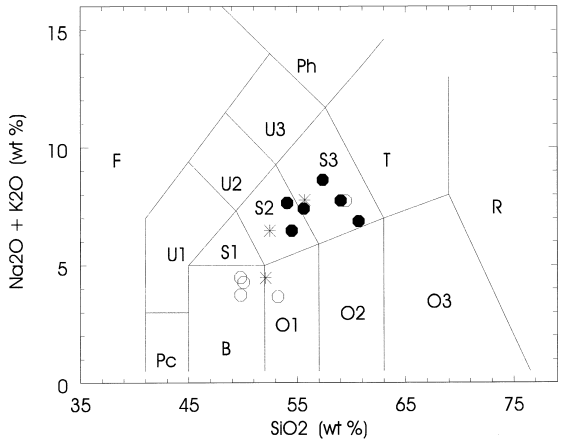

Fig. 2. TAS classification diagram for representative samples of the studied dykes. Pc: picrobasalt; B: basalt; O1: basaltic andesite; O2: andesite; O3: dacite; R: rhyolite; S1: trachybasalt; S2: basaltic trachyandesite; S3: trachyandesite; T: trachyte; F: foidite; U1: tephrite/basanite; U2: phonotephrite; U3: tephriphonolite; Ph: phonolite. Symbols: open circles: normal magnetic fabric, full circles: inverse fabric, asterisks: ill defined fabric. More references in the text.

content is apparent in samples from the southern sector of the studied area, especially in the basaltic trachyandesites. Mafites are altered to chlorite and fine-grained opaque mineral aggregates that in the extreme cases are pseudomorphs of clinoamphibole. Propilitization is not generalized.

Dyke attitudes vary between 260–270°and 300–310° for the trachyandesitic types and 280–290° for the basaltic, andesitic and dacitic dykes, and they are frequently segmented. Their emplacement may be controlled by extensional fractures related to major WNW–ESE strike–slip faults that have been reactivated and are now recognized in the Sierra. Rotation of the far-field generalized W–E compression could account for the strike variations. No clear crosscutting relation has been recognized between the three systems.

TAS classification of the dykes (Le Maitre et al., 1989) allows the identification of two series: Series 1, composed of subalkaline basalts, basaltic andesites and dacites that are located preferentially in the central part of the Sierra de Mamil Choique; and Series 2, composed of alkaline trachyandesites and basaltic trachyandesites, more frequently found in the NW quadrant of the Sierra. Both series plot in the calcalkaline field of the AFM diagram (Fig. 2), but with Series 1 corresponding to medium-K and Series 2 to high-K. Both are metaluminous with only mildly peraluminous compositions in the dacites of Series 1. Harker diagrams show that the main chemical differences between the series are in the LIL, LREE and some HFS elements like Zr and Hf that are more concentrated in Series 2, whereas, CaO, MgO and Al_2O_3 contents are lower. Some correlations between the series and type of magnetic fabric were also found (see below). Higher Fe_2O_3 is associated with higher magnetic susceptibility values and an increase in both is apparent towards the SE sector of the Sierra. Zr/Y vs. Zr diagram locate the samples in the continental arc field. Tectonic classification indicates volcanic arc calc-alkaline basalts or andesites.

K/Ar whole-rock radiometric ages were calculated for two samples, one porphyric basalt (G3, paleomagnetic site D-3) and one andesite (G30, site D-12). Analytical data were obtained at the Centro de Pesquisas Geocronologicas, Instituto de Geociencias, University of Sao Paulo (Brazil). Values are presented in Table 1. These radiometric ages indicate that emplacement of the dykes occurred in the Bajocian–Bathonian, somewhat later than the Marifil Formation, but slightly older that the reported ages for the Lonco Trapial Group. The calculated values are coincident with the age assigned to the Chon-Aike Formation in DM (Pankhurst et al., 1993; Rapela and Pankhurst, 1993).

Table 1
Analytical data for the K/Ar determinations

No.	% K	75% Error	Ar^{40} Rad $\times 10^{-6}$ (ccSTP/g)	Ar (atm)	T_{max} (Ma)	Age	Error 1 (Cox–Darl)	Error 2 (Difer)
G3	1.8233	0.5000	12.50	5.68	171.9	168.4	1.9 (1.1%)	3.5 (2.1%)
G30	1.5364	0.5652	10.81	31.07	177.2	172.7	2.0 (1.2%)	4.5 (2.6%)

4. Paleomagnetic study

Seventy-four oriented block samples were collected at 15 sites (generally five per site), each site corresponding to a single dyke, distributed in different areas of the Sierra de Mamil Choique (Fig. 1). All samples, except those from sites D-10, D-11 and D-12, were oriented both with sun and magnetic compasses. Differences between both readings were generally kept within 3°. However, 15 samples showed differences larger than 5°, with a maximum deviation of 13°, in which cases the magnetic readings were discarded. Two to four cores were subsequently drilled from each sample in the laboratory.

Standard stepwise demagnetization techniques were applied to all specimens collected. Two specimens per site were submitted to a detailed demagnetization either by alternating field (AF) or thermal techniques. This pilot procedure indicated that thermal treatments were less efficient to define the remanence components than the AF method in some cases (Fig. 3A,B). In others, however, both thermal and AF demagnetization provided very similar results (Fig. 3E,F,J,L). Therefore, most of the remaining samples were submitted to stepwise AF demagnetization in 12 to 16 steps up to a maximum field of 140 mT. Measurements were done in a DC squid cryogenic magnetometer (2G 755R), while demagnetization procedures were carried out with a static three axis AF demagnetizer attached to the cryogenic magnetometer and a Schonstedt thermal demagnetizer (TSD-1).

Most samples showed moderate to high NRM intensities: 0.1 to 5 A/m and stable behaviour with linear decay of magnetization (Fig. 3). A large but very soft magnetic component (Fig. 3A,C,D,G) was frequently found with a random direction (although sometimes parallel to the dyke strike). This component, probably viscous or lightning induced, was easily erased with AF fields of 10–20 mT (Fig. 3). A second magnetic component was generally isolated at higher demagnetizing fields. In most cases, this component trended towards the origin and was considered as the characteristic remanent magnetization (ChRM). ChRM was isolated by means of principal component analysis (Kirshvink, 1980), from at least four consecutive cleaning stages at fields higher than 15 mT or temperatures higher than 250°C. Maximum angular deviations for each magnetic component determination were very seldom greater than 10°, and, in most cases, smaller than 5°. Unblocking temperature and coercivity spectra (Fig. 3) suggest that Ti-poor titanomagnetite is the most likely carrier of the remanence at most sites, although hematite seems to be significant in some samples from site D-14 (see Fig. 3I). Hematite is also the possible carrier of a very small high temperature component isolated between 500°C and 700°C in sample D-15-1a2, with an anomalous direction. Fig. 4 shows hysteresis loops for four samples from different sites obtained with a vibrating sample magnetometer at the São Paulo paleomagnetic laboratory. Three of them show a dominant ferrimagnetic signal, while the remaining one seems to be governed by paramagnetic minerals. Values of coercive force (H_c), saturation magnetization (J_s) and saturation remanence (J_{rs}), obtained at maximum fields of 1 T were calculated after subtraction of the paramagnetic contribution. Both H_c and J_{rs}/J_s from sites D-3 and D-5 fall in the pseudo-single-domain (PSD) field for magnetite, while larger PSD (or partial contribution from multidomain (MD)) magnetite predominates at site D-10 (Day et al., 1977). The dominance by a ferrimagnetic mineral phase is also supported by isothermal remanence acquisition curves obtained with a pulse magnetizer (Fig. 5). All samples show saturation at fields under 400 mT. Fig. 5b shows IRM backfield curves after magnetization at fields of 3.5 T. These results indicate a broad range of remanence coercive forces (H_{cr} from 15 to 75 mT). H_{cr} values suggest that remanence is mainly carried by PSD or SD grains in most cases (see, for instance, Cisowski, 1981; Dankers, 1981).

The characteristic remanence has a N–NE moderate to steep upward direction. Three sites presented the antipodal direction (Fig. 6, Table 2). All sites, except D-19, showed an acceptable within-site consistency, although in some cases lower than expected. This could be due to larger orientation errors associated with hand-sampling. Site D-10 was ruled out because it presented a mean direction clearly anomalous with respect to the remaining sites. As mentioned above, samples from this and sites D-11 and D-12 were solely oriented with magnetic compasses. Site D-11 showed the second lowest magnetic susceptibility (see below) suggesting that the

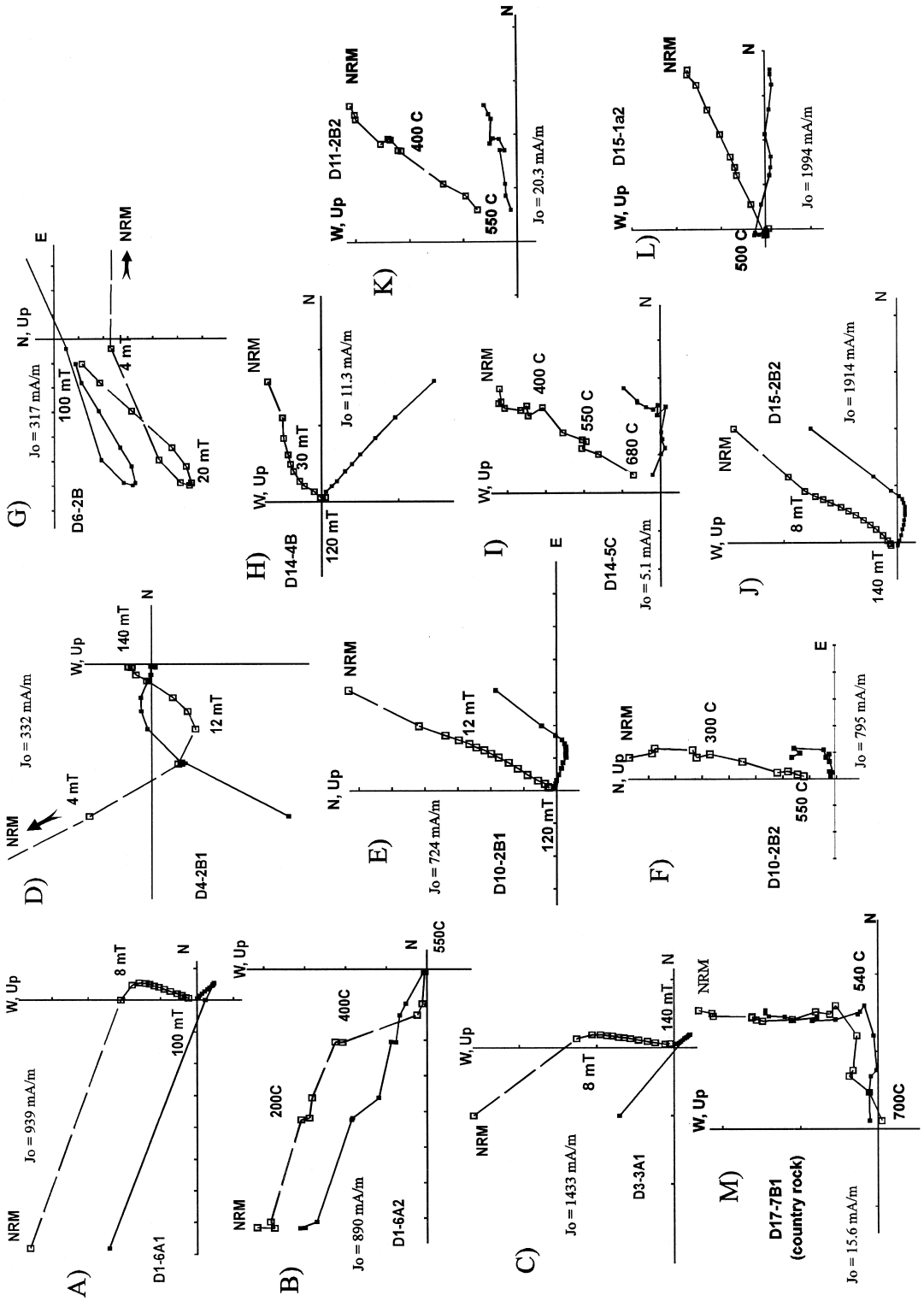
A)
NRM
Jo = 939 mA/m
W, Up
8 mT
100 mT
N
D1-6A1
B)
NRM
Jo = 890 mA/m
W, Up
200C
400C
550C
N
D1-6A2
C)
NRM
Jo = 1433 mA/m
W, Up
8 mT
140 mT
N
D3-3A1
M)
NRM
W, Up
540 C
700C
N
D17-7B1
(country rock)
Jo = 15.6 mA/m
D)
NRM
Jo = 332 mA/m
W, Up
4 mT
140 mT
12 mT
N
D4-2B1
E)
N, Up
Jo = 724 mA/m
NRM
12 mT
120 mT
E
D10-2B1
F)
N, Up
NRM
300 C
550 C
E
Jo = 795 mA/m
D10-2B2
G)
N, Up
E
Jo = 317 mA/m
NRM
100 mT
4 mT
4 mT
20 mT
D6-2B
H)
W, Up
NRM
30 mT
120 mT
N
Jo = 11.3 mA/m
D14-4B
I)
W, Up
NRM
400 C
550 C
680 C
N
D14-5C
Jo = 5.1 mA/m
J)
W, Up
NRM
8 mT
140 mT
N
Jo = 1914 mA/m
D15-2B2
K)
W, Up
NRM
400 C
550 C
N
Jo = 20.3 mA/m
D11-2B2
L)
W, Up
NRM
500 C
N
Jo = 1994 mA/m
D15-1a2

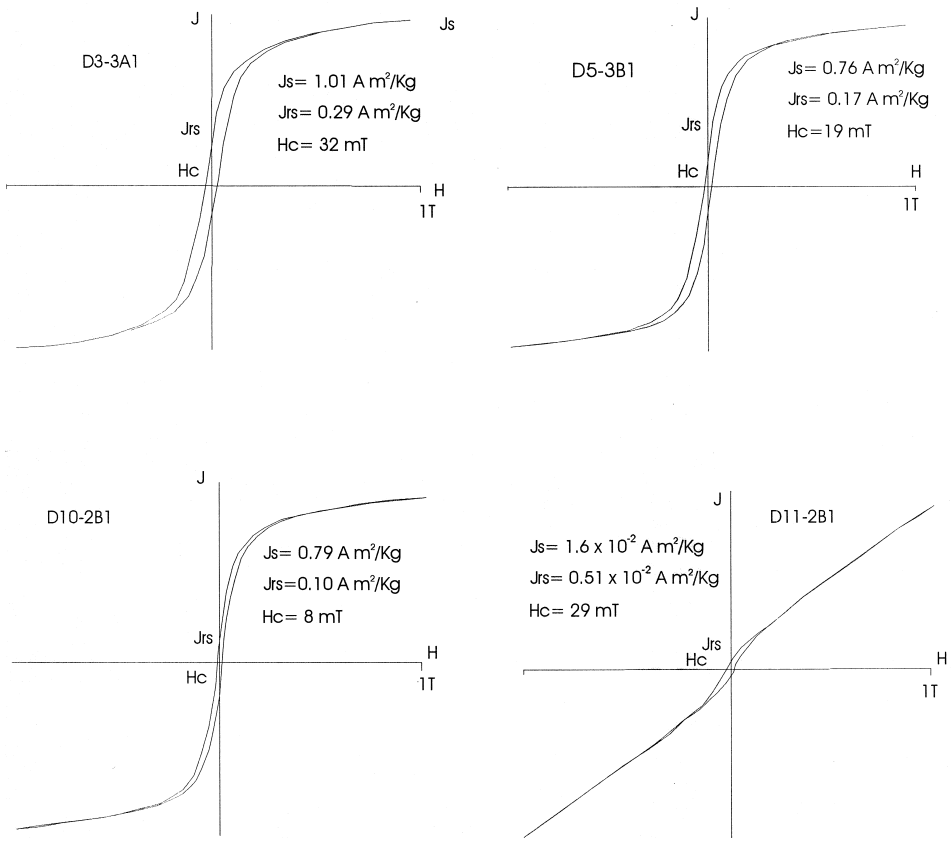

Fig. 4. Hysteresis loops for four samples of the Mamil Choique dykes. Values of J_s (magnetization at 1 T), J_{rs} (magnetic remanence at 1 T) and H_c (coercive force) are calculated after graphically removing the paramagnetic signal. Samples D-3-3A1 and D5-3B1 are consistent with SD to PSD dominance, sample D-10-2B1 is consistent with PSD to MD dominance, sample D-11-2B1 shows a dominance of the paramagnetic fraction. See discussion in the text.

magnetic orientation is probably not affected by local anomalous fields. On the other hand, some of the dispersion of remanence directions from site D-12 may also be assigned to magnetic orientation errors. However, its consistency with mean directions from the remaining sites suggests that their overall influence is likely very small.

A preliminary paleomagnetic study was also carried out on samples from the country rocks (granitoids) collected at four different sites (sites D-2, D-8, D-9 and D-16). They showed varied magnetic behaviours, i.e., multicomponent (D-2, D-8), low coercivities (D-9) and high coercivities and unblocking temperatures (D-16), with no obvious presence of the dykes' characteristic remanence. Two extra block samples were collected from the granite exposed at site D-17 a few centimeters from the contact with the dyke. The aim of this was to perform a contact test. Three cores from these samples were submitted to stepwise thermal demagneti-

Fig. 3. Typical Zijderveld plots from samples of the Mamil Choique dykes submitted to AF or thermal cleaning. Note the removal of very large soft components in some samples and the linear decay of the characteristic remanence towards the origin in most cases. The magnetic behaviour of a sample from the country rock at the intrusive contact in site D-17 is also shown. Full (open) symbols correspond to vector projections on the horizontal (vertical) plane.

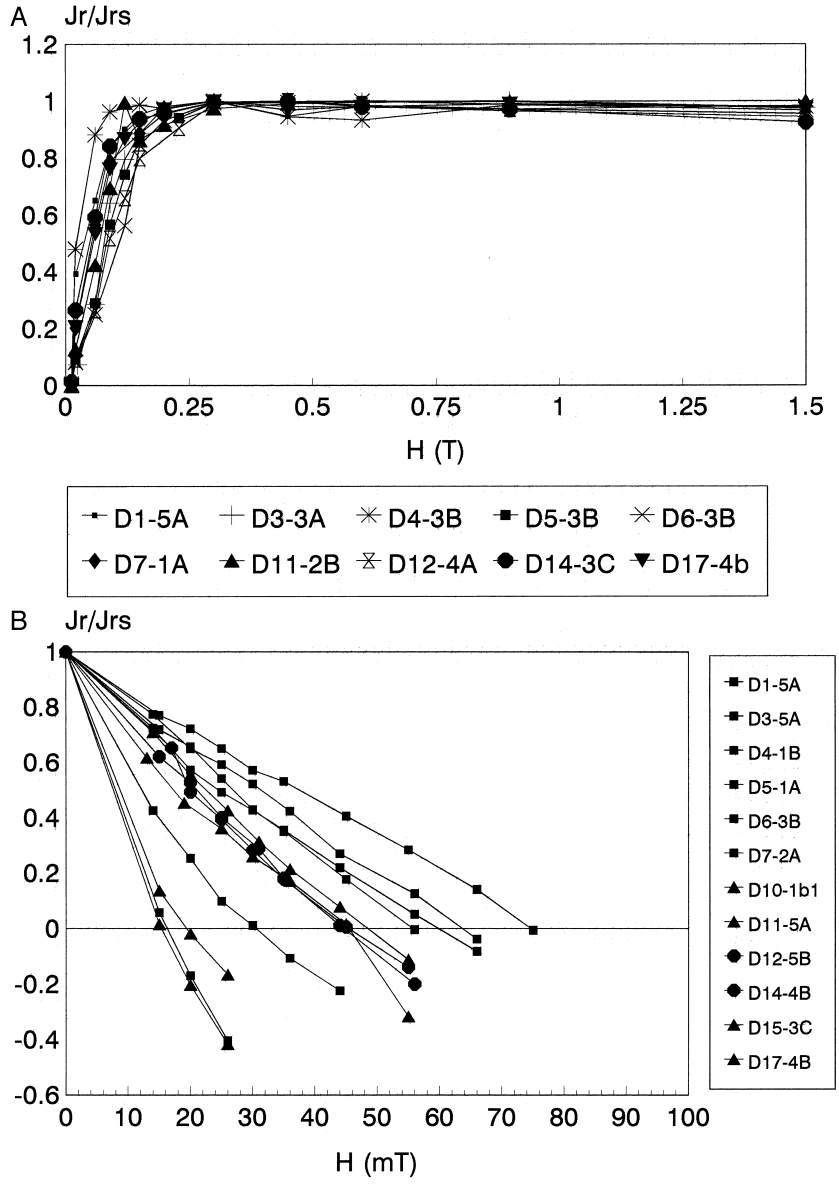

Fig. 5. (A) Representative normalized isothermal remanence acquisition curves for samples of the Mamil Choique dykes. Saturation at fields under 0.4 T suggests that (Ti poor) titanomagnetite is the most likely magnetic carrier. (B) Backfield IRM curves after saturation at 3.5 T. Triangles, squares and circles indicate samples with normal (type I), inverse (type II) and ill-defined (type III) magnetic fabric, respectively.

zation. The magnetic behaviour of one of these samples is shown in Fig. 3M. Two magnetic components are evident, apparently carried by magnetite and hematite, respectively. The direction of the lower temperature component does not agree with those from the dykes, suggesting that the magnetite has not been affected by the intrusion or remagnetized afterwards. The higher temperature remanence is closer to, although shallower than, the ChRM mean direction from site D-17; which may suggest, but cannot prove, that hematite precipitation was related to the intrusion of the dyke. The results of this contact test

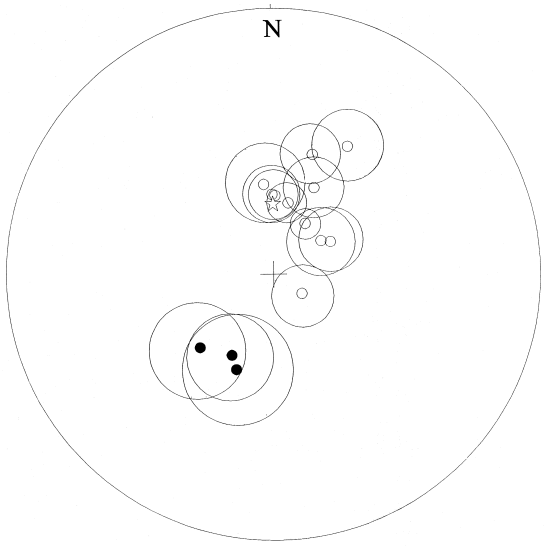

Fig. 6. Mean site characteristic remanence directions and their α_{95} for the Mamil Choique dykes. Open (full) circles indicate projections in the upper (lower) hemisphere. Star indicates the expected direction for an axial geocentric dipole.

cannot prove that the dykes carry a primary thermal remanence, but, together with the results from the other sites in the granitoids, they indicate that a regional remagnetization is unlikely.

Most sampled dykes were observed in the field to be vertical. This and regional geologic considerations allow the interpretation that they were not significantly tilted after intrusion. Therefore, no tectonic correction was applied to the paleomagnetic data. A reversal test (MacFadden and McElhinny, 1990) was applied for the normal and reverse mean site directions yielding a positive reversal test graded as C. This indicates that no significant undetected secondary magnetizations bias the mean remanence directions, and that enough time elapsed during the intrusion of the dykes to permit at least one reversal of the Earth Magnetic Field to take place. This suggests that the paleosecular variation has been sufficiently averaged. At site D-13, both polarities were found at the same site, i.e., specimens from sample D13-4 carried ChRM of reverse polarity.

5. Magnetic fabric results

The magnetic fabric analysis of dyke swarms has proven to be a very useful tool in determining magma emplacement kinematics (Knight and Walker, 1988; Ernst and Baragar, 1992; Raposo and Ernesto, 1995; Glen et al., 1997). However, determination of magma

Table 2
Mean site paleomagnetic data from the Mamil Choique dykes
Dec (declination), Inc (inclination) of the mean characteristic remanence; VGP, virtual geomagnetic pole; α_{95} = radius of 95% confidence circle (Fisher, 1953); n (N) = number of specimens (sites) computed in the mean.

Site (Az, thickness)	n	Dec	Inc	α_{95}	k	VGP (latitude)	VGP (longitude)
D-1 (298°, 1.5 m)	4	32.2°	−64.7°	6.3°	210	66.6°	42.6°
D-3 (298°, 4 m)	7	60.4°	−62.4°	12.8°	24	46.6°	43.6°
D-4 (278°, 1 m)	4	225.7°	47.3°	17.5°	28	−50.8°	194.8°
D-5 (263°, 2.5 m)	8	11.9°	−59.4°	7.6°	55	80.9°	13.7°
D-6 (308°, 5 m)	6	202.1°	47.9°	19.4°	13	−68.0°	171.3°
D-7 (303°, 5 m)	5	354.1°	−52.4°	14.5°	29	80.1°	260.0°
D-10* (303°, 2.5 m)	5	125.1°	−75.4°	12.6°	38	23.2°	85.6°
D-11 (295°, 2 m)	5	359.3°	−56.5°	11.2°	48	85.3°	282.8°
D-12 (267°, 6 m)	6	208.0°	52.1°	16.0°	18	−66.1°	186.7°
D-13 (278°, 2 m)	7	54.9°	−65.4°	13.7°	20	51.4°	47.6°
D-14 (263°, 2 m)	7	25.5°	−50.6°	11.3°	29	67.1°	0.7°
D-15 (301°, 5.5 m)	6	18.5°	−39.4°	10.3°	43	65.1°	333.9°
D-17 (289°, 3 m)	7	1.4°	−57.0°	10.2°	36	85.7°	305.2°
D-18 (288°, 2 m)	4	30.5°	−31.9°	11.7°	62	54.2°	345.9°
Mean directions	$N = 13$	26.0°	−56.9°	7.8°	29		
Mean VGPs	$N = 13$			9.7°	19	−70.2°	190.4°

*Site was not considered in the mean.

Table 3
AMS data from the Mamil Choique dykes (k_{mean} values in 10^{-5} SI)

Site	Sample	k_1 (10^{-5} SI)	Dec (°)	Inc (°)	k_2 (10^{-5}SI)	Dec (°)	Inc (°)	k_3 (10^{-5}SI)	Dec (°)	Inc (°)	P	k_{mean}
D-1	1-5a	2066.62	25	10	2028.69	215	80	1982.22	116	2	1.043	2025.84
	1-5b	2080.18	26	15	2038.24	205	75	1992.89	296	1	1.044	2037.11
	1-6a	1629.66	47	12	1586.33	233	78	1548.65	137	1	1.052	1588.21
	1-6b	1771.84	42	12	1736.04	215	78	1714.31	312	1	1.034	1740.73
D-3	3-1a	2561.23	31	2	2498.06	297	61	2475.45	122	29	1.035	2511.58
	3-2b	804.719	32	9	774.57	125	17	772.31	274	71	1.042	783.87
	3-3a	1679.77	270	31	1647.87	56	55	1641.47	170	16	1.023	1656.37
	3-4a2	1642.97	239	23	1614.21	351	42	1605.42	128	39	1.023	1620.87
	3-5b	2360.27	37	17	2299.36	283	54	2277.00	138	31	1.037	2312.21
D-4	4-1a	3141.51	201	17	3101.57	48	71	3067.03	294	8	1.024	3103.37
	4-2a2	2556.21	204	34	2534.23	47	54	2512.75	301	11	1.017	2534.40
	4-3b	852.95	185	3	841.02	61	84	833.23	276	5	1.024	842.40
	4-4-1a	1318.80	10	9	1291.29	120	64	1282.12	276	24	1.029	1297.41
D-5	5-1a	993.99	1	24	985.58	262	19	975.03	137	59	1.019	984.87
	5-2a	2202.65	21	8	2151.53	274	63	2125.15	114	25	1.036	2159.78
	5-3b	1694.09	353	17	1666.59	260	9	1648.63	143	71	1.028	1669.77
	5-4a	2821.60	194	0	2707.68	284	18	2696.63	104	72	1.046	2741.97
	5-5a	2650.79	15	1	2549.43	110	82	2520.16	285	8	1.052	2573.46
D-6	6-1a	2457.61	197	14	2434.88	50	74	2413.03	289	9	1.018	2435.17
	6-2b	1448.42	40	42	1425.18	224	48	1415.26	132	2	1.023	1429.62
	6-3b	1269.31	184	48	1258.64	1	42	1252.36	92	1	1.013	1260.10
	6-4a1	1431.84	74	34	1419.91	207	45	1400.19	325	26	1.023	1417.31
	6-5b	1964.76	190	20	1953.71	300	45	1919.04	83	39	1.024	1945.84
D-7	7-1b	1673.87	58	11	1638.58	174	66	1633.05	324	21	1.025	1648.50
	7-2b	1443.89	40	7	1417.52	271	78	1413.38	131	9	1.022	1424.93
	7-3a	2621.52	206	20	2566.01	113	9	2538.38	1	68	1.033	2575.30
	7-4a	1254.37	130	45	1250.10	268	36	1240.68	16	22	1.011	1248.38
	7-5a	1503.68	48	33	1487.10	202	54	1476.68	309	12	1.018	1489.15
D-10	10-1a	2821.10	237	8	2787.31	330	17	2763.07	122	72	1.021	2790.50
	10-2b1	2138.46	284	16	2110.46	41	58	2094.76	186	27	1.021	2114.56
	10-3a	1296.57	267	47	1281.25	124	36	1271.20	19	19	1.020	1283.00
	10-4a2	2472.06	266	15	2428.60	0	14	2420.56	132	69	1.021	2440.41
	10-5a	2937.41	283	10	2921.71	57	76	2869.08	191	10	1.024	2909.40
D-11	11-1b	1255.87	94	14	1237.16	338	61	1213.42	191	25	1.035	1235.48
	11-2b1	79.17	286	7	78.64	186	51	77.82	21	38	1.017	78.54
	11-3a	198.42	191	28	197.99	314	46	194.87	82	31	1.018	197.10
	11-4a	250.65	118	13	249.54	283	76	243.69	27	4	1.028	247.96
	11-5b	168.59	131	27	167.66	248	41	165.74	18	36	1.017	167.33
D-12	12-1a	4782.34	206	11	4730.10	114	13	4709.87	334	73	1.015	4740.77
	12-2b	4165.15	110	79	4105.24	306	10	3981.39	215	3	1.046	4083.93
	12-3b	2861.67	186	4	2802.26	96	8	2787.82	301	81	1.026	2817.25
	12-4b	2304.13	7	2	2250.25	100	45	2233.42	275	45	1.032	2262.60
	12-5b1	3754.56	11	54	3711.48	122	15	3657.97	221	32	1.026	3708.00
D-13	13-1b	1973.80	36	2	1957.10	128	46	1941.15	304	44	1.017	1957.35
	13-2b	2203.65	127	43	2171.75	320	46	2139.22	223	7	1.030	2171.54
	13-3a	2116.23	149	30	2085.96	306	58	2060.34	53	10	1.027	2087.51
	13-4a	2056.57	148	4	2021.66	248	70	1989.75	57	20	1.034	2022.66
	13-5a	2204.66	327	2	2160.07	233	62	2122.14	58	28	1.039	2162.29
D-14	14-1b	54.02	189	53	53.57	56	27	52.51	313	23	1.029	53.37
	14-2b	70.13	137	23	67.37	41	14	66.24	283	62	1.059	67.92
	14-3c	69.56	304	18	67.09	75	63	63.77	208	19	1.091	66.81
	14-4b	56.29	146	30	55.64	357	56	51.84	244	14	1.086	54.59
	14-5b	60.35	236	3	60.01	140	64	58.99	327	26	1.023	59.79

Table 3 (*continued*)

Site	Sample	k_1 (10^{-5} SI)	Dec (°)	Inc (°)	k_2 (10^{-5}SI)	Dec (°)	Inc (°)	k_3 (10^{-5}SI)	Dec (°)	Inc (°)	P	k_{mean}
D-15	15-1a	2125.03	300	32	2108.19	204	10	2094.51	99	56	1.015	2109.24
	15-2b1	2015.13	297	53	1976.94	162	28	1971.04	59	22	1.022	1987.70
	15-3c	2142.61	284	57	2106.81	136	29	2089.73	38	15	1.025	2113.05
	15-4a	2198.50	281	44	2168.11	130	42	2158.56	26	15	1.018	2175.06
D-17	17-1b	1612.08	279	6	1604.16	32	75	1577.28	187	14	1.022	1597.84
	17-2c	2977.98	248	1	2919.45	158	29	2908.52	339	60	1.024	2935.31
	17-3c	2648.53	134	1	2625.42	39	82	2597.91	224	8	1.019	2623.95
	17-4b	191.77	274	50	190.66	122	36	186.20	22	14	1.030	189.54
	17-5a	2782.29	91	0	2745.62	348	88	2696.13	181	1	1.032	2741.35
D-18	18-1b	4916.23	29	54	4867.50	147	18	4813.12	248	29	1.021	4865.62
	18-2a2	5222.19	0	16	5124.35	99	29	5085.29	245	56	1.027	5143.95
	18-3b	4692.92	330	10	4610.40	81	64	4583.52	236	23	1.024	4628.95
	18-4a	5160.78	15	38	5064.69	135	32	5028.65	251	35	1.026	5084.71
	18-5c	5147.34	44	57	5058.54	138	3	4993.61	230	33	1.031	5066.49
D-19	19-1a	8840.61	289	26	8809.21	176	39	8721.16	43	40	1.014	8790.32
	19-2b	8308.69	141	7	8260.84	259	76	8213.11	50	13	1.012	8260.88
	19-3a	7347.22	156	57	7325.87	288	28	7268.22	39	17	1.011	7313.77
	19-4a	3414.44	20	22	3314.71	111	3	3286.83	207	67	1.039	3338.66
	19-5a1	5100.74	3	32	4910.08	110	26	4849.16	231	47	1.052	4953.33

flow direction from anisotropy of magnetic susceptibility (AMS) measurements is not straightforward. Rochette et al. (1992) demonstrated that AMS is generally a complex phenomenon due to the mixed contributions of different magnetic minerals and domain states to the overall anisotropy of a sample. It is well known that single-domain (SD) magnetite has an inverse magnetic fabric (Potter and Stephenson, 1988). This means that if this mineral dominates the magnetic susceptibility of a sample, its AMS should show an inverse fabric, i.e., maximum axis (k_1) perpendicular to the dyke plane, as opposite to the normal fabric in which the minimum axis (k_3) should be normal to the dyke plane. Partial contributions of SD and PSD or MD magnetite may yield intermediate fabrics, with the intermediate axis (k_2) normal to the dyke plane and k_1 and k_3 on the plane.

Magnetic fabric measurements were carried out with a Minisep anisotropy meter at the Instituto Astronomico e Geofisico (São Paulo, Brazil). Four or five 2.2-cm-high specimens obtained from different paleomagnetic samples were measured for each site, before any magnetic cleaning was applied.

Most sites were characterized by high bulk magnetic susceptibility (k). Mean site values were generally between 10^{-2} and 3×10^{-2} SI (Table 3). Sites D-18 and D-19 (located to the SE) showed higher values, around 6×10^{-2} SI. All these values are typical of k governed by the ferromagnetic fraction (Tarling and Hrouda, 1993). Two other sites, on the other hand, showed lower mean susceptibilities, D-11: 2×10^{-3} SI and D-14: 5×10^{-4} SI, suggesting important contributions from the paramagnetic minerals.

Anisotropy degree ($P = k_1 / k_3$) was generally low, with most samples yielding values between 1.02 and 1.04, and, in very few cases, over 1.06. This is to say that differences between the high and low-k axes were generally below 4%. This is consistent with previous measurements on basic dykes (Knight and Walker, 1988). No correlation was observed between P and k. The shape of the AMS ellipsoid shows no consistent pattern, with no significant tendency towards either an oblate or a prolate fabric (Fig. 7), similar to what Knight and Walker (1988) found in the Hawaiian basic dykes.

The distribution of AMS maximum, intermediate and minimum axes at each site (dyke) are presented in Fig. 8. The strike of the dyke at each site is indicated for comparison with the anisotropy data. Distribution of AMS axes can be grouped into three categories: type I, normal fabric: well-defined oblate or prolate fabric with k_3 (minimum) normal to the dyke plane; type II, inverse fabric: well-defined

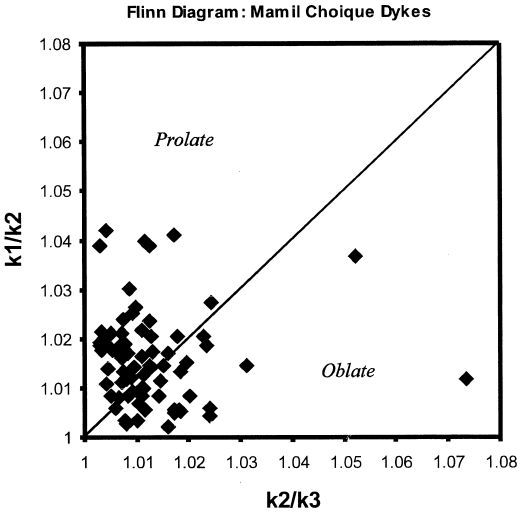

Fig. 7. Foliation (k_2/k_3) vs. lineation (k_1/k_2) diagram to indicate the shape of the anisotropy of magnetic susceptibility ellipsoid. The oblate and prolate fabric fields are indicated.

oblate or prolate fabric with k_3 in the dyke plane and type III: ill-defined fabric, with no consistent orientation of axes.

Type I is represented by sites D-10, D-11, D-13(?), D-15, D-17 and D-18(?). Some of these sites also show one or two cases of axis exchange (k_3 replaced by k_2). Type-II fabric is shown by sites D-1, D-3, D-4, D-5, D-7, D-13(?) and D-18(?). D-13 and D-18 appear in both groups as they could either be an inverse or a normal fabric rotated 40–50° from the dyke plane. D-6, D-12, D-14 and D-19 correspond to type III.

It can be inferred from Fig. 4 that samples from sites D-3, D-5 and D-10 are characterized by the dominance of ferrimagnetic minerals (magnetite?) with minor contributions from paramagnetic phases. On the other hand, paramagnetic contribution to the bulk susceptibility is very significant (about 60%) in the sample from site D11. This correlates with lower

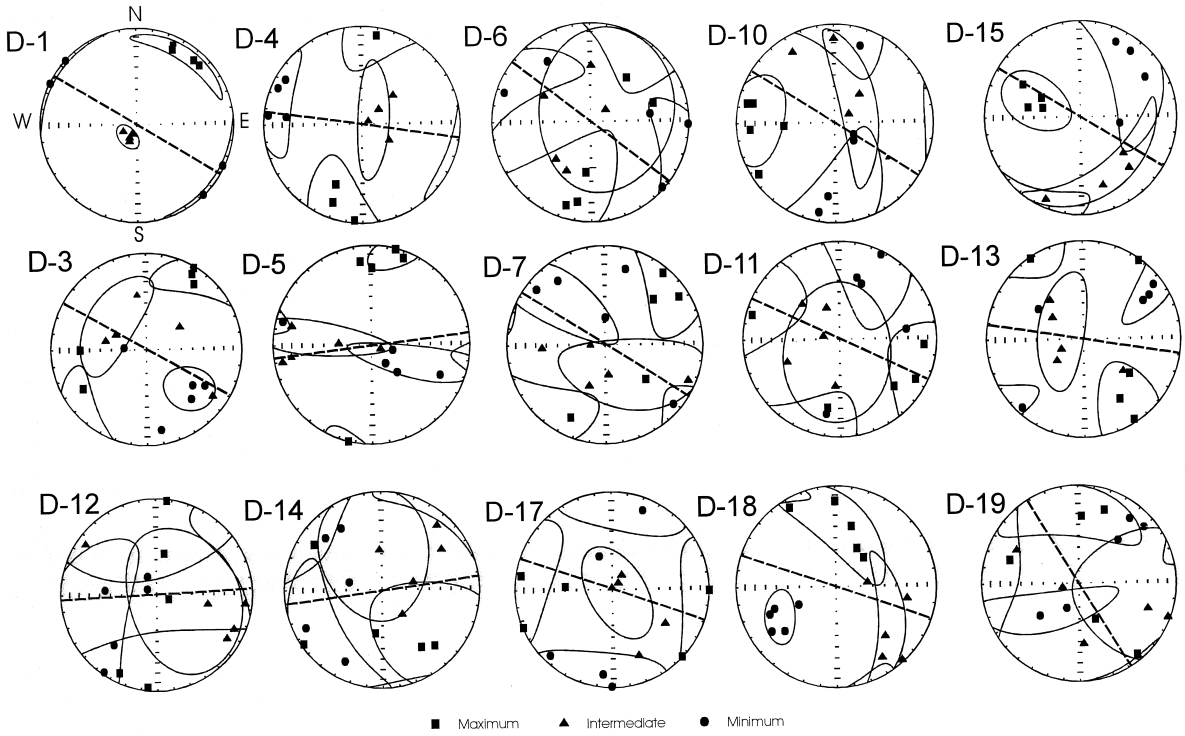

Fig. 8. Distribution of axes of maximum (k_1), intermediate (k_2) and minimum (k_3) anisotropy of magnetic susceptibility for each sample at each site. Ellipses of 95% confidence (Jelinek, 1978) for each axis and the dyke plane are depicted with continuous and dashed lines, respectively.

k values at this site. As already mentioned, both H_c and J_{rs}/J_s suggest dominance of SD or PSD magnetite at sites D-3 and D-5, while large PSD (or MD) magnetite predominates at site D-10 (Day et al., 1977). The magnetic fabric at the first two sites correspond to type II (inverse fabric), while at site D10 the fabric is normal (type I). The dominance of paramagnetic minerals at site D-11 corresponds also to a normal fabric. Microscopic observations suggest that biotite is probably the most important contributor to the paramagnetic signal at this site, which is consistent with the normal fabric produced by this mineral (Rochette et al.,1992). As already mentioned, results from IRM backfield curves (Fig. 5b) indicate a broad range of remanence coercive forces. In the figure, different symbols were assigned to samples from sites with magnetic fabric types I, II and III. Although the ranges of H_{cr} are broad for both types I and II, those samples with inverse magnetic fabric show higher H_{cr} values than those with normal fabric.

On this basis, we interpret that the inverse magnetic fabric found in several dykes is probably due to the dominance of SD magnetite. It is interesting to note that most inverse fabrics are found in the dykes located in the NW area of the Sierra de Mamil Choique. This suggests some systematic petrological differences of the dykes, with smaller grain size of the ferrimagnetic fraction as we move from SE to NW. The petrologic signature is also evident in the TAS diagram of Fig. 2 where type-I and -II samples tend to plot in different fields of the diagram indicating a significant compositional variation between samples with different magnetic fabric types. A mineralogical cause may be not the only explanation for the inverse magnetic fabric (Rochette et al., 1999), both anisotropy of distribution and secondary fabrics have been suggested as alternate mechanisms. However, the facts that the anisotropy degree P is slightly higher in those samples with inverse fabric ($P = 1.032$) than in those with normal fabric ($P = 1.025$), and that it has no relation with the bulk susceptibility k, suggest that none of these explanations is the most likely one.

Type-I sites would be the most suitable for determination of flow direction during dyke emplacement, i.e., k_1 directions. However, only a fraction of the dykes sampled showed normal fabric. Furthermore, as Tauxe et al.(1998) have recently shown, unambiguous determination of flow direction in dykes can only be accomplished by systematic sampling of opposite borders of the dyke, which is not our case. This precludes any reliable determination in these dykes and suggests that many previous determinations should be re-evaluated.

6. Interpretation of the paleomagnetic results

A virtual geomagnetic pole (VGP) was computed from each mean-site remanence direction (Table 2). Their average is the paleomagnetic pole for the Mamil Choique basic to intermediate dykes: DM, 70.2°S, 190.4°E, $N = 13$, $\alpha_{95} = 9.7°$.

The Jurassic South American apparent polar wander path was recently analyzed by Vizán (1993) and Iglesia Llanos (1996, 1997), who suggested a rapid southward drift of South America in the late Early and Middle Jurassic. The position of the DM pole is shown in Fig. 9, together with other Early to Middle Jurassic poles from South America. The DM pole is particularly coincident with the paleomagnetic pole from the Chon-Aike lavas at Estancia La Reconquista (LR, Vilas, 1974). The Chon-Aike Group was recently dated by Pankhurst et al. (1993) as 168 ± 2 Ma (Rb/Sr isochrone). This age is coincident with that obtained for the Mamil Choique dykes (168–172 Ma). This suggests a temporal correlation between the intrusion of the Mamil Choique dykes and the extrusion of the Chon-Aike lavas. Thus, DM and LR may indicate the c. 170 Ma pole for South America. However, the radiometric ages obtained by Pankhurst et al. (1993) correspond to samples collected near Puerto Deseado, and it is not clear if they can be extrapolated to the rocks exposed in Estancia La Reconquista. Furthermore, an old paleomagnetic study on Chon-Aike lavas exposed in Puerto Deseado (Valencio and Vilas, 1970) yielded a pole (PD, Fig. 9A) not coincident with DM and LR. Iglesia Llanos (1997) and Vizán (1998) have recently recomputed some of the Middle Jurassic poles. These new modified pole positions are shown in Fig. 9B. These authors computed an overall pole for the Chon-Aike lavas slightly different from the previous mean pole computed by Vilas (1974). They also presented a marginally different position for the Mar-

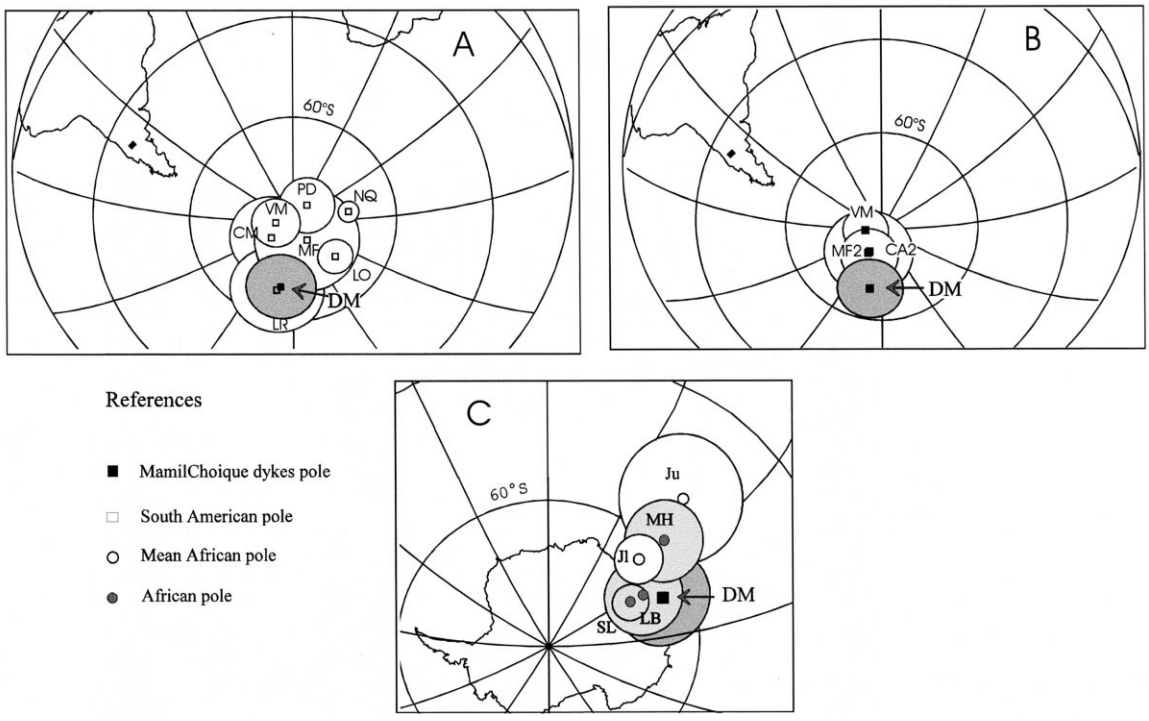

Fig. 9. (A) Paleomagnetic pole of the Mamil Choique dykes (DM, c. 170 Ma) with its 95% confidence circle (grey). Other Early and Middle Jurassic paleomagnetic poles from South America are shown: NQ: Rajapalo-Chacay Melehue, c.190 Ma (Iglesia Llanos, 1996); LO: Lepá-Ostarena, c. 187 Ma (Vizán, 1993); MF: Marifil, c. 183 Ma (Mena, 1990; recomputed by Rapalini et al., 1993); CM: Camarones, c. 178 Ma (Creer et al., 1972); VM, Maranhao c. 175 Ma (Schult and Guerreiro, 1979); PD, Chon-Aike, Pto Deseado, c. 168 Ma (Valencio and Vilas, 1970); LR, Chon-Aike, La Reconquista c. 168 Ma? (Vilas, 1974). (B) Comparison of position of DM with recently recomputed Middle Jurasic poles from South America (Iglesia Llanos, 1997; Vizán, in press). CA2: recomputed pole for Chon-Aike formation; MF2: recomputed polo for Marifil Formation; VM: Maranhao volcanics (Schult and Guerreiro, 1979). (C) Comparison of position of DM after rotation to southafrican coordinates (Lottes and Rowley, 1990) with Early and Late Jurassic mean poles for Africa (J_l and J_u, Van der Voo, 1993, also rotated to South African coordinates) and the paleomagnetic poles from the Mateke Hills ring complexes (MH, 169–177 Ma, Gough et al., 1964), the Lebombo basalts (LB, 173–183 Ma, Hentorn, 1981) and the Stormberg lavas (SL, 175–185 Ma, Kosterov and Perrin, 1996).

ifil pole. When plotted against these poles, the DM pole is somewhat discordant, although its 95% confidence circle partially overlaps those of the Marifil and Chon-Aike poles. To further investigate the possibility of DM being a reliable Middle Jurassic paleomagnetic pole for South America, it was compared with coeval poles from Africa (Fig. 9C). To accomplish this, DM was rotated to South African coordinates according to the parameters of Lottes and Rowley (1990). The use of a different paleoreconstruction does not modify substantially the results. In Fig. 9C, DM is shown together with the mean Early and Late Jurassic poles for Africa computed by Van der Voo (1993) rotated also to South African coordinates. These poles correspond to the 195–177 and 176–145 Ma time spans, respectively. DM partially agrees with the Early Jurassic mean pole, but is not consistent with the Upper Jurassic pole. Since the mean poles comprise periods of 20 to 30 Ma and might average out some polar wander, the comparison was also made with individual African poles. Three poles were selected as the most reliable for the Middle Jurassic: MH (Mateke Hills ring complexes, 169–177 Ma, Gough et al., 1964), LB (Lebombo basalts, 173–183 Ma, Hentorn, 1981) and SL (Stormberg lavas, 175–185 Ma, Kosterov and Perrin, 1996). DM agrees well with the latter two but does not agree so well with the first. This may suggest

that the Mamil Choique dykes are coeval with the Stormberg lavas and the Lebombo basalt, although this would imply a slightly older age for them than that obtained in our study. Therefore, comparison with the African data does not give an unambiguous answer to our dilemma. On the other hand, DM may indicate some minor clockwise rotation of the study area. Since the area is located close to the Gastre Fault System (see Rapela and Pankhurst, 1992) for which major dextral displacement were postulated during the Late Triassic–Middle Jurassic, some late in situ clockwise tectonic rotation may have occurred. However, since the reference pole is problematic any tectonic consideration of the DM position should await new Middle Jurassic paleomagnetic data from Patagonia and the rest of South America.

7. Conclusions

The first systematic study on Middle Jurassic dyke swarms from Patagonia is reported. Results include: petrological characterization, radiometric dating, magnetic fabric and paleomagnetic data.

Two whole-rock K/Ar determinations indicate that these dykes were intruded around 170 Ma (Middle Jurassic).

An AMS study on 15 dykes showed that they carry different kinds of magnetic fabric (i.e., normal and inverse fabric), apparently governed by compositional differences. The normal (inverse) magnetic fabric was assigned to a dominance of PSD–MD (SD) magnetite.

A paleomagnetic study of these dykes allowed us to determine that most of them have a ChRM carried by Ti-poor titanomagnetite. This is confirmed by some rock-magnetic experiments. The characteristic remanence showed opposite polarities at different sites, indicating that emplacement of these dykes spanned at least one polarity reversal of the Earth Magnetic Field. A paleomagnetic pole, computed by averaging VGPs from each individual dyke, is not substantially apart from other Middle Jurassic poles from South America. However, further refinement of the Jurassic South American apparent polar wander path is needed to evaluate whether or not the Mamil Choique dykes were affected by a small tectonic rotation.

Acknowledgements

This study was made possible by financial support of the Fundación Antorchas (Argentina) to A.E.R. Institutional support by the University of Buenos Aires and the Consejo Nacional de Investigaciones Científicas y Técnicas (CONICET, Argentina) are acknowledged. Paleomagnetic measurements were done at the Laboratorio de Paleomagnetismo Daniel Valencio (University of Buenos Aires). Marcia Ernesto kindly facilitated the instruments at the paleomagnetic laboratory of the Instituto Astronomico e Geofisico (University of Sao Paulo, Brasil) for carrying out the AMS and hysteresis measurements. A.E.R. is particularly indebted to all personnel at that lab for their help in getting used with the equipments. S. Truco collaborated during the field work. Thorough reviews by two anonymous referees substantially improved the final version of the paper.

References

Alric, V.I., Haller, M.J., Féraud, G., Bertrand, H., Zubia, M., 1996. Cronología $^{40}Ar/^{39}Ar$ del volcanismo Jurásico de la Patagonia extrandina. Actas del Congreso Geologico Argentino, 13th 5, 243–250, Buenos Aires.

Beck, M.E. Jr., 1988. Analysis of Late Jurassic — recent paleomagnetic data from active plate margins of South America. Journal of South American Earth Sciences 1, 39–52.

Cerredo, M.E., López de Luchi, M.G., 1998. Mamil Choique Granitoids, southwestern North Patagonian Massif, Argentina: magmatism and metamorphism associated with a polyphasic evolution. Journal of South American Earth Sciences 11, 499–515.

Cisowski, S., 1981. Interacting vs. non-interacting single domain behaviour in natural and synthetic samples. Physics of the Earth and Planetary Interiors 26, 56–62.

Creer, K.M., Mitchell, J.G., Abou Deeb, J., 1972. Palaeomagnetism and radiometric age of the Jurassic Chon-Aike Formation form Santa Cruz province, Argentina: implications for the opening of the South Atlantic. Earth and Planetary Science Letters 14, 131–138.

Dalla Salda, L., Varela, R., Cingolani, C., Aragón, E., 1994. The Río Chico Paleozoic Crystalline Complex and the evolution of Northern Patagonia. Journal of South American Earth Sciences 7, 1–10.

Dankers, P., 1981. Relationship between median destructive field

and remanent coercive forces for dispersed natural magnetite, titanomagnetite and hematite. Geophysical Journal of the Royal Astronomical Society 64, 447–461.

Day, R., Fuller, M., Schmidt, V.A., 1977. Hysteresis properties of titanomagnetites: grain size and compositional dependence. Physics of the Earth and Planetary Interiors 13, 260–267.

Ernst, R.E., Baragar, W.R.A., 1992. Evidence from magnetic fabric for the flow pattern of magma in the McKenzie giant radiating dyke swarm. Nature 356, 511–513.

Glen, J.M.G., Renne, P.R., Milner, S.C., Coe, R.S., 1997. Magma flow inferred from anisotropy of magnetic susceptibility in the Coastal Paraná-Etendeka igneous province: evidence for rifting before flood volcanism. Geology 25, 1131–1134.

Gough, D.I., Brock, A., Jones, D.L., Opdyke, N.D., 1964. The palaeomagnetism of the ring complexes at Marangudzi and the Mateke hills. Journal of Geophysical Research 69, 2499–2507.

Hentorn, D.I., 1981. The magnetostratigraphy of the Lebombo Group along the Olifants river, Kruger National Park. Annals of the Geological Survey (South Africa) 15 (2), 1–10.

Iglesia Llanos, M.P., 1996. Paleomagnetismo y magnetoestratigrafía del Pliensbaquiano–Toarciano (Jurásico) de la Cuenca Neuquina. Revista de la Asociacion Geologica Argentina 51, 339–354.

Iglesia Llanos, M.P., 1997. Magnetoestratigrafía y Paleomagnetismo del Jurásico Inferior marino de la Cuenca Neuquina, República Argentina. PhD Thesis, University of Buenos Aires, Argentina, 337 pp.

Irving, E., Irving, G.A., 1982. Apparent polar wander paths Carboniferous through Cenozoic and the assembly of Gondwana. Geophysical Surveys 5, 141–188.

Jelinek, V., 1978. Statistical processing of magnetic susceptibility measured in groups of specimens. Studia Geophysica et Geodaetica 22, 50–62.

Kirshvink, J.L., 1980. The least-squares line and plane and the analysis of palaeomagnetic data. Geophysical Journal of the Royal Astronomical Society 62, 699–718.

Knight, M.D., Walker, G.P.L., 1988. Magma flow directions in dikes of the Koolau complex Oahu, determined from magnetic fabric studies. Journal of Geophysical Research 93, 4301–4319.

Kosterov, A.A., Perrin, M., 1996. Paleomagnetism of the Lesotho basalt, southern Africa. Earth and Planetary Science Letters 139, 63–78.

Lesta, P., Ferello, R., 1972. Región extrandina de Chubut y Norte de Santa Cruz. In: Leanza, A.F. (Ed.), Geología Regional Argentina, Academia Nacional de Ciencias, Córdoba, Argentina. pp. 601–654.

Le Maitre, R.W., Bateman, P., Dudek, A., Kelelr, J., Lameyre, J., Le Bas, M.J., Sabine, P.A., Schmid, R., Sorensen, H., Streckeisen, A., Woolley, A.R., Zanettin, B., 1989. In: A Classification of the Igneous Rocks and Glossary of Terms. Blackwell, Oxford, p. 193.

López de Luchi, M.G., Cerredo, M.E., 1996. Metamorphism, deformation and related magmatism in the Río Chico area. Actas del Congreso Geologico Argentino, 13th 5, 533, Buenos Aires.

López de Lucchi, M., Rapalini, A.E., 1997. Jurassic dyke swarms in the Sierra de Mamil Choique, North Patagonian Massif: lithology, age and paleomagnetism. In: Simposio Final IGCP Proj. 345, Lithospheric Evolution of The Andes. VIII Cong. Geológico Chileno, Resumenes Expandidos. pp. 1679–1683.

Lottes, A.L., Rowley, D.B., 1990. Reconstruction of the Laurasian and Gondwanan segments of Permian Pangaea. Memoir — Geological Society 12, 383–395.

MacFadden, P.L., McElhinny, M.W., 1990. Classification of the reversal test in palaeomagnetism. Geophysical Journal International 103, 725–729.

Mena, M., 1990. Correlación paleomagnética de diversos afloramientos del Complejo Marifil (provincia de Rio Negro). Revista de la Asociacion Geologica Argentina 45, 136–144.

Nullo, F., 1978. Descripción geológica de la Hoja 41d, Lipetrén, Provincia del Río Negro. Boletin del Servicio Geologico Nacional (Buenos Aires) 158, 88 pp.

Page, R., Page, S., 1993. Petrología y significado tectónico del Jurásico volcánico del Chubut Central. Revista de la Asociacion Geologica Argentina 48, 41–58.

Pankhurst, R.J., Rapela, C.R., 1995. Production of Jurassic rhyolites by anatexis of the lower crust of Patagonia. Earth and Planetary Science Letters 134, 23–36.

Pankhurst, R.J., Sruoga, P., Rapela, C.W., 1993. Estudio geocronológico Rb–Sr de los complejos Chon-Aike y El Quemado a los 47°30′ L.S. Actas del Congreso Geologico Argentino, 12th 4, 171–178, Actas del Congreso de Exploracion de Hidrocarburos, 2nd.

Potter, D.K., Stephenson, A., 1988. Single-domain particles in rocks and magnetic fabric analysis. Geophysical Research Letters 15, 1097–1100.

Rapalini, A.E., Abdeldayem, A.L., Tarling, D.H., 1993. Intracontinental movements in Western Gondwanaland: a palaeomagnetic test. Tectonophysics 220, 127–139.

Rapela, C.W., Pankhurst, R.J., 1992. The granites of northern Patagonia and the Gastre Fault System in relation to the break-up of Gondwana. In: Storey, B.C, Alabaster, T., Pankhurst, R.J. (Eds.), Magmatism and the Causes of Continental Break-up 68 Geological Society of London, UK, pp. 209–220, Special Publication.

Rapela, C.W., Pankhurst, R.J., 1993. El volcanismo riolítico del noreste de la Patagonia: un evento meso-jurásico de corta duración y origen profundo. Actas del Congreso Geologico Argentino, 12th 4, 179–188, Actas del Congreso de Exploracion de Hidrocarburos, Buenos Aires, 2nd.

Raposo, M.I.B., Ernesto, M., 1995. Anisotropy of magnetic susceptibility in the Ponta Grossa dyke swarm (Brazil) and its relationship with magma flow direction. Physics of the Earth and Planetary Interiors 87, 183–196.

Ravazzoli, I., Sesana, F.L., 1977. Descripcion geológica de la Hoja 41c, Río Chico, Provincia de Río Negro. In: Boletin del Servicio Geologico Nacional (Buenos Aires, Argentina) 148, 80 pp.

Rochette, P., Aubourg, C., Perrin, M., 1999. Is this magnetic fabric normal? A review and case studies in volcanic formations. Tectonophysics 307, 219–234.

Rochette, P., Jackson, M., Aubourg, C., 1992. Rock magnetism and the interpretation of anisotropy of magnetic susceptibility. Reviews of Geophysics 30, 209–226.

Schult, A., Guerreiro, S.D.C., 1979. Palaeomagnetism of Mesozoic igneous rocks from the Maranhao Basin, Brazil, and the timing of the opening of the South Atlantic. Earth and Planetary Science Letters 42, 427–436.

Tauxe, L., Gee, J.S., Staudigel, H., 1998. Flow directions in dikes from anisotropy of magnetic susceptibility data: the bootstrap way. Journal of Geophysical Research 103, 17775–17790.

Valencio, D.A., Vilas, J.F., 1970. Palaeomagnetism of some Middle Jurassic lavas from south-east Argentina. Nature 225, 262–264.

Van der Voo, R., 1993. Paleomagnetism of the Atlantic, Tethys and Iapetus Oceans. Cambridge Univ. Press, Cambridge, 411 pp.

Vilas, J.F., 1974. Palaeomagnetism of some igneous rocks of the middle Jurassic Chon-Aike Formation from Estancia La Reconquista, Province of Santa Cruz, Argentina. Geophysical Journal of the Royal astronomical Society 39, 511–522.

Vizán, H., 1993. Marco geológico y paleomagnetismo-de unidades de la Cuenca Liásica del Oeste del Chubut (Argentina). PhD Thesis, University of Buenos Aires, Argentina, 200 pp.

Vizán, H., 1998. Paleomagnetism of the Lepá and Osta Arena Formations (Lower Jurassic), Patagonia, Argentina. Journal of South American Earth Sciences 11, 33–50.